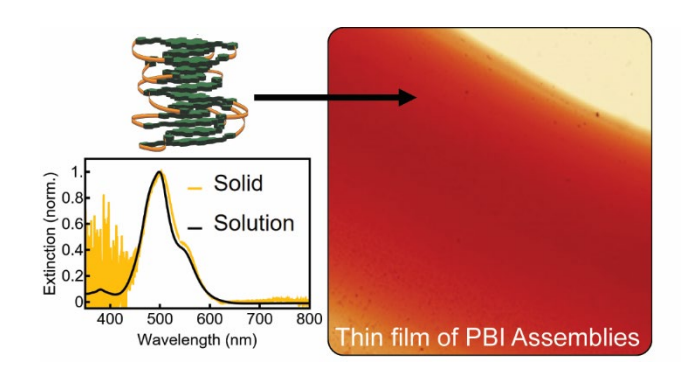
# Covalently tethered assemblies improve energetic homogeneity and exciton transport in organic materials

Alexander J. King<sup>1,2</sup>, Victor A. Paulino<sup>3</sup>, Skyler R. Hollinbeck<sup>1</sup>, Ifigeneia Tsironi<sup>3</sup>, Jarek A. Maleszka<sup>3</sup>, Jean-Hubert Olivier<sup>3\*†</sup>, Erik M. Grumstrup<sup>1,2\*</sup>

AUTHOR ADDRESS 1. Department of Chemistry and Biochemistry, Montana State University, Bozeman, Montana 59717 United States; 2. Montana Materials Science Program, Montana State University, Bozeman, Montana 59717; 3. Department of Chemistry, University of Miami, Coral Gables, Florida 33146, United States.



ABSTRACT: Structural and functional heterogeneity is a consequence of the weak non-covalent interactions that direct formation of organic materials from solution precursors. While covalent tethering of solution-phase assemblies provides a compelling strategy to enhance intermolecular order, the effects of this tethering strategy on the formed solid-state materials remain unestablished. This work uses pump-probe microscopy to compare excited-state dynamics in thin films fabricated from tethered perylene bisimide assemblies to those from non-covalent assemblies. On average, tethered films exhibit faster and more homogeneous excited state lifetimes, consistent with stronger and more uniform intermolecular coupling. Optical measurements of excited-state diffusion show that the tethered film has ~75% faster transport than the control film. Kinetic Monte Carlo modeling suggests that reduction of site energetic disorder is sufficient to quantitatively explain the difference in diffusion coefficients. These results provide strong support that covalent tethering is a promising strategy to enhance the structural and energetic ordering in molecular materials.

The diverse application portfolio of organic semiconductors in photovoltaics,1 chemosensors,2 flexible electronics,3 and light-emitting diodes<sup>4</sup> is in part enabled by their sensitive structure-function relationship, which provides a means to tune functionality via synthetic modification. However, this same structure-function sensitivity can be problematic in molecular materials, as minor variation in short- and long-range structural order can cause significant differences in functional properties at nano to mesoscale dimensions.<sup>5</sup> Because solid-state organic materials typically rely on non-covalent interactions to enforce intermolecular ordering, minor perturbations to, for example, solvent dielectric constant<sup>6</sup>, temperature<sup>7</sup>, and molecular concentration8 will inherently change the structure and defect density of the bulk material. These minor changes to the crystal structure can cause significant differences in electrical and optical properties, 9-14 thus making semiconducting materials derived from organic building blocks prone to unpredictable func-

Materials derived from the family of perylene-3,4,9,10-tetracarboxylic bisimide (perylene bisimide, PBI) are promising organic semiconductors as they exhibit strong chemical, thermal, and photo stability, 9, 15 as well as high electron mobility and fluorescence quantum yields. 16, 17 Self-assembly of the perylene core can produce structurally well-defined nanoscale objects. 18- 21 If robustly translated to the solid state, such bottom up design strategies could be leveraged to, for example, engineer materials with non-equilibrium structures aimed at specific functionalities. 21, 22 Despite the promise, a robust and predictable approach for translating the well-defined structure of solvated self-assembled precursors into a solid-state material remains challenging. 23

One strategy to overcome this challenge is to reinforce the weak non-covalent interactions of solution-phase assemblies so that their structure is resistant to perturbation. Recently, Olivier and coworkers have developed a covalent tethering/stapling approach, whereby self-assembled supramolecular assemblies of perylene bisimide chromophores are covalently tethered to rigidify the  $\pi$ -stacked structures.<sup>24, 25</sup> Compared to conventional molecular assemblies that are bound only by van der Waals interactions, the structures of the covalently-tethered assemblies are significantly more resistant to changes in temperature and dielectric environment in the solution phase. As a result, the

electronic coupling between adjacent units is less sensitive to the local environment.<sup>24</sup>

While this previous work demonstrates the validity of the covalent tethering strategy to enhance interchromophoric coupling in solvated assemblies, there is to date, no work that addresses how the functionality of tethered assemblies, engineered in solution, translates from the solution phase to a solid-state material. Based on the structural robustness exhibited by the solution-phase tethered assemblies, we hypothesized that the electronic structure determined by the solution-phase self-assembly process would be maintained upon condensation into the solid-state. We further anticipated that materials formed from a suspension of the tethered assemblies would be characterized by greater long-range electronic ordering relative to materials formed from non-covalent assemblies, and, therefore, exhibit 1) more homogeneous excited state behavior, and 2) faster exciton diffusion.

To test these hypotheses, we used ultrafast pump-probe microscopy (PPM) to compare excited state dynamics in a film cast from PBI non-covalent assemblies to a film comprised of

covalently-tethered PBI assemblies PBI-Stap-2 Because PPM provides the ability to measure ultrafast spatiotemporal dynamics with spatial resolution better than 1 um, it is possible to compare excited state decay kinetics from different locations on the same film. We find that excited state decay lifetimes are faster and significantly more uniform in the thin films formed from tethered assemblies, relative to decay kinetics collected on the untethered film. We also use PPM to directly measure exciton diffusion in the two films and find that excited state transport in the tethered-assembly film is significantly faster than in the untethered film. Kinetic Monte Carlo (kMC) modeling of exciton transport suggests that reduction of energetic disorder is sufficient to explain the approximate two-fold increase in exciton diffusion observed. Together, these results provide strong support that covalent tethering enforces the structure and electronic coupling of solution phase supramolecular assemblies, and therefore provides a promising approach for achieving optimized solid-state organic materials for future electronic and optoelectronic needs.

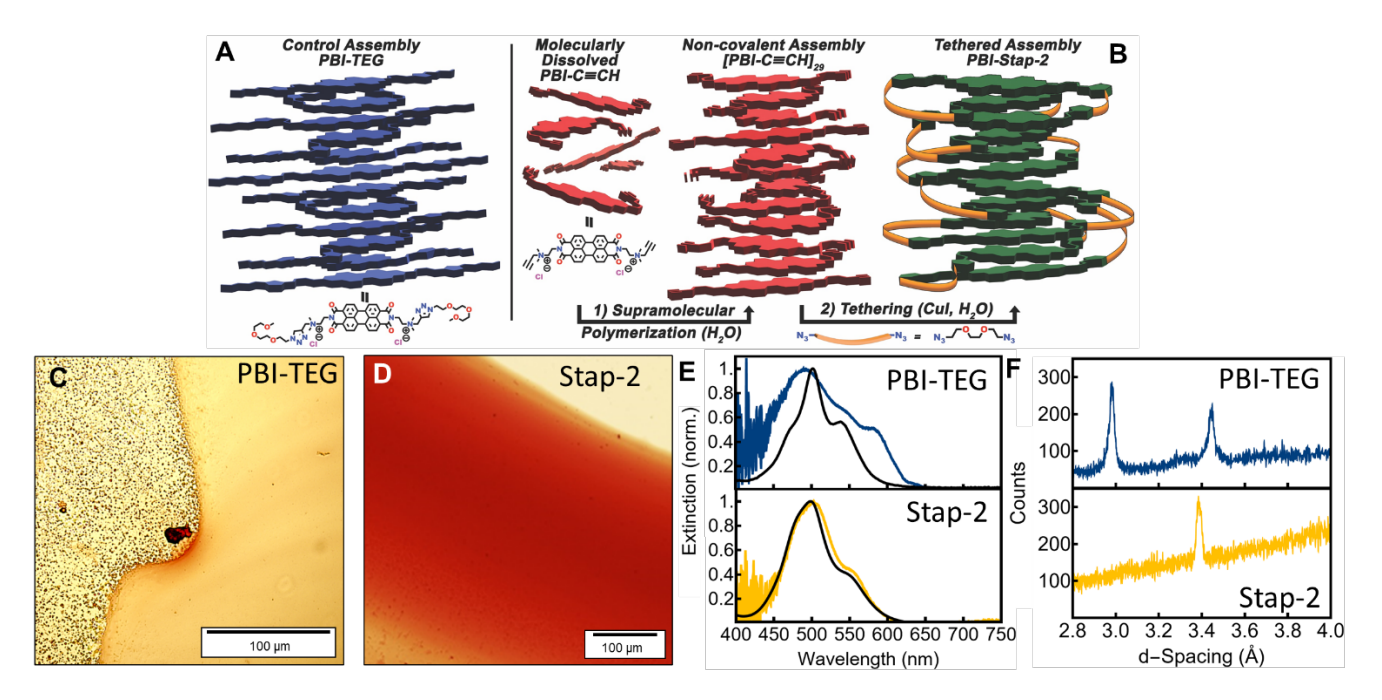


Figure 1: Summary of precursors and thin films. A) Schematic of the control precursor PBI-TEG B) Synthetic scheme to generate tethered superstructures (PBI-Stap-2) by aggregation followed by covalent tethering. C) and D) bright field microscope images of the PBI-TEG and PBI-Stap-2 films, respectively. E) Comparison of absorption spectra for the precursor solutions (black) and the deposited thin films (yellow/blue) for the two systems. F) Comparison of the XRD patterns from films prepared from the PBI-TEG and PBI-Stap-2 precursors.

Figure 1 summarizes the composition of the two PBI systems compared in this letter. Panels A and B show schematic representations of the solution-phase control (PBI-TEG, PBI-trieth-ylene glycol) and tethered assemblies (PBI-Stap-2) used as precursors for the two films. PBI-Stap-2 features ethylene oxide linkers that tether the PBI core with triazole functionality. The short molecular tether has been shown to create tethered structures whose excitonic coupling remain virtually unperturbed in solution as a function of solvent temperature and dielectric constant.<sup>24</sup> The control PBI-TEG is functionalized with analogous ethylene oxide terminal groups. The synthesis and characterization of both precursors have been reported previously.<sup>24, 25</sup> Briefly, tethered assemblies are synthesized from the reaction

of the parent supramolecular polymer with the linker precursor  $N_3(CH_2CH_2O)_2N_3$  in water. Due to the polymeric character of these assemblies, gel permeation chromatography is used to remove unreacted species and narrow the size distribution of the PBI-Stap-2 assemblies.

To prepare films of the PBI-TEG (Fig. 1C) and PBI-Stap-2 (Fig. 1D), aqueous solutions were prepared and drop-cast onto borosilicate slides. It is important to highlight that careful control of environmental parameters and advanced fabrication techniques like printing or meniscus-guided coating can provide a significant handle for controlling the structure of solution-processed organic thin films.<sup>26, 27</sup> Here, we aim to demonstrate that despite using a fabrication approach that provides

minimal control over the environmental variables, films with highly uniform electronic structure can be formed if morphology is enforced at an appropriate length scale.

Visible absorption spectra of the control and tethered assembly films were collected with a homebuilt microscopic spectrometer. The spectrum of the PBI-TEG film (Fig. 1E-Blue) is characterized by three overlapping transitions at 495, 545, and 585 nm. Based on comparison to the absorption spectrum of the assembly precursor solution (solid black), the transitions at 495 and 545 nm are assigned to the 0-1 and 0-0 vibronic transitions.<sup>24</sup> The distinct shoulder at 585 nm is unique to solid-state films of PBI-TEG, and likely derives from low-energy states formed as a result of structural disorder introduced during film condensation. While a bathochromic shift could indicate formation of local J-type or HJ-type aggregation<sup>28-30</sup>, fluorescence spectroscopy and microscopy performed on the PBI-TEG film showed no detectable emission, which would be expected in the case of J-type coupling. In contrast to the control film, the tethered PBI-Stap-2 film exhibits a ground state absorption spectrum (Fig. 1E-gold) nearly identical to that of the solution-phase assemblies (black), indicating that the electronic structure is preserved upon formation of the solid-state film.

To characterize the structure of the films, we next turned to grazing incidence x-ray diffraction (Fig. 1F). The XRD pattern

from the PBI-TEG film reveals two distinct peaks at  $2\theta = 25.85^{\circ}$ (3.45 Å) and  $2\theta = 29.90^{\circ} (2.98 \text{ Å})$ . We assign the 3.45 Å peak to the  $\pi$ - $\pi$  stacking distance, but the assignment of the peak at 2.98 Å is less certain. It is unlikely to arise from a polymorph with a closer packing as it falls outside the range of 3.4 Å to 3.6 Å observed for the  $\pi$ - $\pi$  stacking distance in PBI materials.<sup>31-34</sup> Instead we assign it to a diffraction plane that is non-coplanar with the PBI core, reflecting long range symmetry in crystal directions orthogonal to the  $\pi$ - $\pi$  stacking direction.<sup>35</sup> For the PBI-Stap-2 film, we observe only a single diffraction peak at  $2\theta$  = 26.30° (3.39 Å), which is expected for a film comprised of columnar  $\pi$ -stacked assemblies. The smaller spacing associated with this peak indicates that covalent tethering enforces a more tightly packed  $\pi$ – $\pi$  stack than the PBI-TEG film. The peak from the PBI-Stap-2 film is also narrower than the corresponding peak in the PBI-TEG film, particularly near the base, indicating that PBI-Stap-2 film is structurally more homogeneous along the  $\pi$ -stacking direction. Note that in the PBI-TEG film there is a weak feature near 3.3 Å that may indicate a small population of the closer packing arrangement seen in the Stap-2 film, however, this feature is broad and poorly resolved.

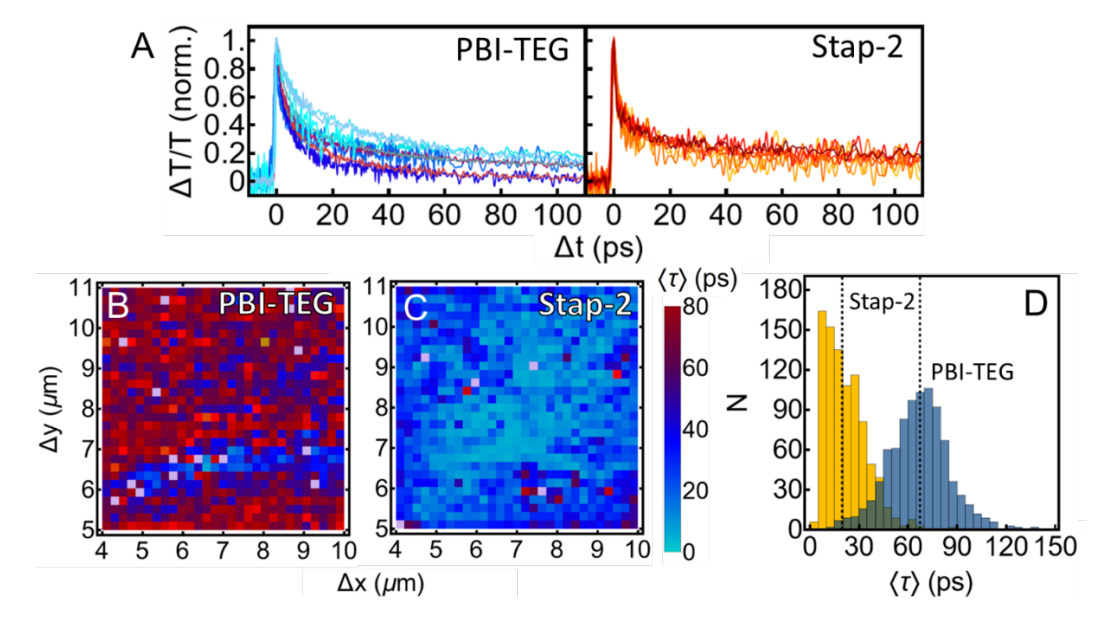


Figure 2: Excited state lifetimes of the two thin films. (A) Kinetics of the PBI-TEG and PBI-Stap-2 films measured at different locations on each film. Excited state average lifetime images of the control PBI-TEG film (B) and the PBI-Stap-2 film (C). (D) Distribution of average lifetimes from each of the lifetime images in panels B and C. The dashed lines show the mean lifetimes of 68.4 and 23.8 ps for the control PBI-TEG and PBI-Stap-2 films, respectively.

The closer interchromophore distance observed in XRD suggests that the electronic coupling should be altered in the PBI-Stap-2 film. To compare the ultrafast dynamics of the two films and evaluate the impact of covalent tethering, we utilized ultrafast pump-probe microscopy (PPM), which provides the ability to measure ultrafast dynamics with sub-micron spatial resolution and directly image exciton transport.<sup>30, 36-38</sup> Both films were excited at 500 nm, near the peak of the 0-1 vibronic transition (Fig. 1E) with an excitation fluence limited to 130 μJ/cm² to eliminate nonlinear recombination processes contributing to the kinetics.<sup>39</sup> The probe wavelength of 800 nm monitors a broad photoinduced absorption, which has previously been assigned to a mixed Frenkel exciton, charge-transfer state in the solution

phase assemblies.<sup>24</sup> Broadband transient absorption spectra of the thin films (Supporting Information, SI) are consistent with this spectral assignment and show that the PBI-Stap-2 excited state exhibits greater charge transfer character than the PBI-TEG film.

Because pump-probe microscopy has sub-micron spatial resolution, it provides the opportunity to characterize the excited state lifetime in a manner inaccessible to conventional time-resolved spectroscopies. By measuring decay kinetics at several locations on each film, we find that excited state dynamics in different locations of PBI-TEG are significantly more heterogeneous than those of the PBI-Stap-2 (Fig. 2A). We observed similar behavior across two additional films of both PBI-TEG and

PBI-Stap-2 prepared on different days, indicating that the differences in excited state lifetime behavior are systematic to the precursor materials and fabrication approach employed. To visualize this difference in behavior, we collected pump-probe images over a 6×6 µm region of each film for a series of increasing time delays. We fit the resultant kinetics from each spatial pixel of the image stack to a biexponential model to extract an average lifetime for that location on the films. Figures 2B and 2C average excited state lifetime  $(a_1\tau_1 + a_2\tau_2)/(a_1 + a_2)$  images for PBI-TEG and PBI-Stap-2 films, respectively. When the images are compared (scaling is identical), the PBI-TEG film shows significantly longer-lived and more widely distributed excited state lifetimes relative to the film of the locked PBI-Stap-2 assemblies.

Histograms of the 900 locations probed in the lifetime images are shown in Fig. 2D. From these distributions, two material differences are apparent. First, the average lifetime of the control PBI-TEG film is 69 ps, whereas the PBI-Stap-2 film has a significantly shorter average lifetime of 23 ps. Second, the distribution of lifetimes shows more variation in the control film than the PBI-Stap-2 film. ( $\sigma_{TEG} = 29 \ ps$ ;  $\sigma_{Stap-2} = 16 \ ps$ ). While it is difficult to assign a specific mechanism with single wavelength measurements, the rapid excited state relaxation observed in the PBI-Stap-2 film is characteristic of strong intermolecular coupling, 40-43 which activates fast excited state relaxation pathways through charge transfer state mixing, 44-46 strong dipole-dipole coupling, 47 and/or internal conversion. 48 The narrower lifetime distribution observed for the PBI-Stap-2 tethered film further suggests that intermolecular coupling is more homogeneous than in the control PBI-TEG film. Although there are sites on the control film that exhibit a similar lifetime as the PBI-Stap-2 film, there are many more sites with longer lifetimes, which likely derive from a combination (depending on the local morphology) of states with weaker intermolecular coupling and from energetically low-lying trap states.

Without high resolution broadband<sup>22, 39</sup> or multi-dimensional time-resolved microscopies<sup>49</sup>, it is difficult to assign which specific mechanisms, for example Frenkel-CT exciton mixing<sup>50, 51</sup>, excimer stabilization<sup>52</sup>, and/or geometric rearrangement/selftrapping<sup>53</sup>, are responsible for the longer lifetimes observed in the control film. However, since the films are chemically homogeneous, the variability in lifetime observed from site to site in the PBI-TEG film must reflect morphological defects and differences in intermolecular coupling. Regardless of their nature, the heterogeneity observed clearly highlights one of the primary challenges of characterizing and ultimately utilizing organic materials – the functional properties are highly sensitive to microscopic morphology changes that are an intrinsic characteristic of film fabrication. Our results indicate that covalent tethering is a promising strategy for mitigating such heterogeneity and achieving films with significantly improved electronic homogeneity, even under minimally controlled fabrication conditions.

To determine the effects of covalent tethering on excited state transport, we next turned to spatially offset pump-probe microscopy. For these measurements, the probe beam is positioned at a fixed location and the pump beam is scanned over the probe to generate an image of the excited state spatial distribution (Fig. 3A) as a function of the delay time,  $\Delta t$ . By collecting a series of images at increasing  $\Delta t$  between 0 and 150 ps, excited state transport can be measured with precision that is limited only by signal-to-noise levels. The averaged 1D images are fit by numerical convolution of the diffusion kernel with the initial

( $\Delta t = 0$  ps) spatial profile to determine the mean squared deviation (MSD) of the excited state profile.<sup>55</sup> Linear fits to the MSD provide a measure of the diffusion coefficient (Fig. 3B).

Figure 3C, D shows diffusion coefficients measured in 12 locations on the control PBI-TEG film and 15 locations on the PBI-Stap-2 tethered film. On average, the diffusion coefficient of the control film is measured to be  $1.12 \pm 0.38$  cm<sup>2</sup>s<sup>-1</sup>. The PBI-Stap-2 film exhibits nearly 75% faster transport, with an average diffusion coefficient of  $1.94 \pm 0.48$  cm<sup>2</sup>s<sup>-1</sup>. These average values are similar to diffusion coefficients measured in comparable, well-ordered organic materials<sup>56</sup> but slower than observed in vapor-deposited PBI films on the 0-3 ps timescale, which have been reported to exceed 40 cm<sup>2</sup>/s.<sup>57</sup> For both films, we observe significant variability in observed transport rates. Although measurement noise is likely responsible for some of the observed variation, microscale morphology differences are also likely contributors to the width of the distribution for both films. For the control film, the presence of well-resolved peaks in the X-ray diffraction pattern indicates that well-ordered domains are present but overall that the film is less ordered than PBI-Stap-2. The lifetime imaging data presented in Fig. 2 is another indicator of microscale morphological heterogeneity. For the PBI-Stap-2 film, lifetime imaging suggests that, at least from the perspective of excited state relaxation, the film is more homogeneous than the control film. These results are consistent with a narrowed density of states, suggesting that relative to the control film, the PBI-Stap-2 film is likely to have a reduced density of localized trap sites that inhibit transport. Instead, we attribute the site-to-site variation in measured diffusion coefficient to variability in inter-assembly coupling due to differences in the geometrical alignment of adjacent assemblies.

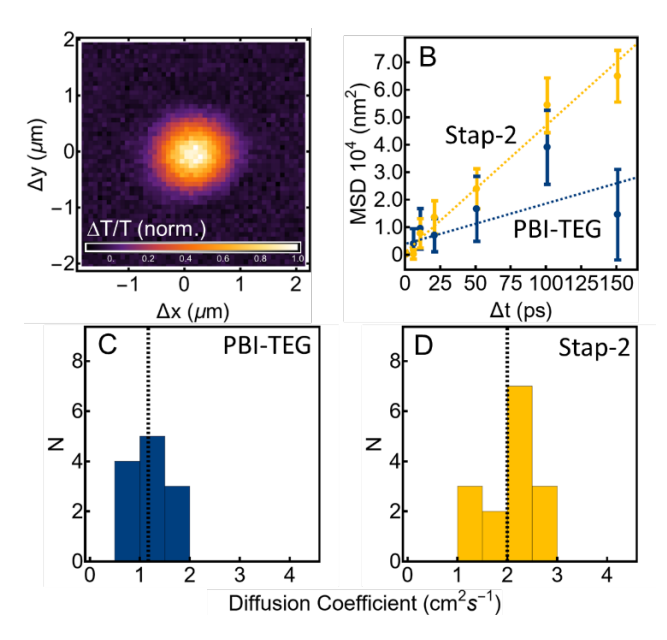


Figure 3: Comparison of excited state transport. A) Diffusion spot measured on the PBI-Stap-2 film at  $\Delta t = 0$  ps. C) Representative mean squared deviation data collected for PBI-TEG (Blue,  $0.83 \pm 0.29 \text{ cm}^2\text{s}^{-1}$ ) and PBI-Stap-2 (Yellow,  $2.06 \pm 0.17 \text{ cm}^2\text{s}^{-1}$ ). Distributions of measured diffusion coefficients for PBI-TEG (C) and PBI-Stap-2 (D) with average values (indicated by dashed lines) of  $1.12 \pm 0.38 \text{ cm}^2\text{s}^{-1}$  and  $1.94 \pm 0.48 \text{ cm}^2\text{s}^{-1}$ , respectively.

Despite the site-to-site variability observed for both films, the difference in transport rates is significant at the 0.01 confidence

level (P < 0.005 using the Mann-Whitney test), suggesting that covalent tethering improves exciton transport, likely by narrowing the density of states and reducing trapping. To provide further insight into this hypothesis, we use a kinetic Monte Carlo (kMC) approach to model transport in the films, where the probability of inter-site hopping is parameterized using a Miller-Abrahams model (further detail available in supporting information). We generate a 3D cubic grid, with each site assigned an energy based on a Gaussian distribution of variable energetic width. Exciton trajectories are propagated and mean square displacements are used to calculate average diffusion constants (SI).

We first parameterize the model to reproduce the experimentally observed diffusion coefficient for PBI-TEG of ~1.1 cm²s¹. Then, to model the Stap-2 film, all parameters are kept identical, except for the width of the energetic distribution. We find that by reducing the width from ~75 meV for PBI-TEG to ~50 meV for PBI-Stap-2, the model quantitatively reproduces the experimentally observed diffusion coefficient of ~1.9 cm²s¹ in PBI-Stap-2 (SI). Given the likely importance of both coherent and incoherent transport mechanisms, <sup>57, 59</sup> as well as the potential role played by polarons<sup>60</sup> and charge transfer states<sup>61</sup>, the simple kMC model described above is unlikely to capture the full mechanistic complexity of transport in these materials. Nevertheless, because the two films are nearly chemically identical, using the model as a comparative tool provides insight into the role played by energetic disorder on transport.

In summary, a direct spectroscopic comparison between thin film formed from non-covalent assemblies and from covalently tethered molecular assemblies indicates that interchromophore coupling is enhanced in the covalently tethered film. By using pump-probe microscopy, we provide direct evidence of functional properties that are strongly impacted by this additional ordering: a 73% increase in excited state transport compared to the control film, as well as a shorter and more homogenous excited state lifetime. KMC modeling suggests that narrowing the distribution of site energies, presumably by enhancing structural homogeneity, is an important factor responsible for the observed increase in the transport rate. These results suggest that covalently locking non-covalent assemblies is a promising strategy for reducing structural and energetic heterogeneity in organic functional materials. Combining covalent tethering with well-established solution-based fabrication approaches may be a compelling strategy for designing hierarchical structures into solid-state organic materials.

## **ASSOCIATED CONTENT**

**Supporting Information**. Details of synthesis and sample preparation, experimental details for XRD, description of pump-probe microscope, detailed description of KMC modeling, broadband transient absorption spectra. This material is available free of charge via the Internet at http://pubs.acs.org.

# AUTHOR INFORMATION

## Corresponding Author

\*JHO: jholivier67@unm.edu; EMG: erik.grumstrup@montana.edu

#### Present Addresses

† Department of Chemistry and Chemical Biology; University of New Mexico, 300 Terrace St NE, Albuquerque, New Mexico 87131

#### **Author Contributions**

The manuscript was written through contributions of all authors. / All authors have given approval to the final version of the manuscript.

## **ACKNOWLEDGMENT**

Synthesis and structural characterization of the tethered PBI-Stap-2 assemblies (JHO, VAP, IT, JM) supported by NSF CAREER Award 1941410. Thin film characterization and spectroscopy (AJK, SRH, and EMG) supported by NSF-2154448. EMG and JHO acknowledge the Arnold and Mabel Beckman Foundation.

#### **ABBREVIATIONS**

PBI; perylene bisimide, TEG; triethylene glycol, Stap-2, Stapled-2; KMC, kinetic Monte Carlo

#### REFERENCES

- (1) Kozma, E.; Catellani, M. Perylene diimides based materials for organic solar cells. *Dyes and Pigments* **2013**, *98*, 160-179. DOI: <a href="https://doi.org/10.1016/j.dyepig.2013.01.020">https://doi.org/10.1016/j.dyepig.2013.01.020</a>.
- (2) Zhou, W.; Liu, G.; Yang, B.; Ji, Q.; Xiang, W.; He, H.; Xu, Z.; Qi, C.; Li, S.; Yang, S.; et al. Review on application of perylene diimide (PDI)-based materials in environment: Pollutant detection and degradation. *Science of The Total Environment* **2021**, *780*, 146483. DOI: https://doi.org/10.1016/j.scitotenv.2021.146483.
- (3) Root, S. E.; Savagatrup, S.; Printz, A. D.; Rodriquez, D.; Lipomi, D. J. Mechanical Properties of Organic Semiconductors for Stretchable, Highly Flexible, and Mechanically Robust Electronics. *Chemical Reviews* **2017**, *117*, 6467-6499. DOI: 10.1021/acs.chemrev.7b00003.
- (4) Li, G.; Zhao, Y.; Li, J.; Cao, J.; Zhu, J.; Sun, X. W.; Zhang, Q. Synthesis, Characterization, Physical Properties, and OLED Application of Single BN-Fused Perylene Diimide. *The Journal of Organic Chemistry* **2015**, *80*, 196-203. DOI: 10.1021/jo502296z.
- (5) Brixner, T.; Hildner, R.; Köhler, J.; Lambert, C.; Würthner, F. Exciton Transport in Molecular Aggregates From Natural Antennas to Synthetic Chromophore Systems. *Advanced Energy Materials* **2017**, 7, 1700236. DOI: 10.1002/aenm.201700236.
- (6) Korevaar, P. A.; Schaefer, C.; De Greef, T. F. A.; Meijer, E. W. Controlling Chemical Self-Assembly by Solvent-Dependent Dynamics. *Journal of the American Chemical Society* **2012**, *134*, 13482-13491. DOI: 10.1021/ja305512g.
- (7) Herkert, L.; Droste, J.; Kartha, K. K.; Korevaar, P. A.; De Greef, T. F. A.; Hansen, M. R.; Fernández, G. Pathway Control in Cooperative vs. Anti-Cooperative Supramolecular Polymers. *Angewandte Chemie International Edition* **2019**, *58*, 11344-11349. DOI: 10.1002/anie.201905064.
- (8) Fennel, F.; Wolter, S.; Xie, Z.; Plötz, P.-A.; Kühn, O.; Würthner, F.; Lochbrunner, S. Biphasic Self-Assembly Pathways and Size-Dependent Photophysical Properties of Perylene Bisimide Dye Aggregates. *Journal of the American Chemical Society* **2013**, *135*, 18722-18725. DOI: 10.1021/ja409597x.
- (9) Yang, D.; Ma, D. Development of Organic Semiconductor Photodetectors: From Mechanism to Applications. *Advanced Optical Materials* **2019**, 7, 1800522. DOI: 10.1002/adom.201800522.
- (10) Coropceanu, V.; Cornil, J.; Da Silva Filho, D. A.; Olivier, Y.; Silbey, R.; Brédas, J.-L. Charge Transport in Organic Semiconductors. *Chemical Reviews* **2007**, *107*, 926-952. DOI: 10.1021/cr050140x.
- (11) Troisi, A.; Orlandi, G.; Anthony, J. E. Electronic Interactions and Thermal Disorder in Molecular Crystals Containing Cofacial Pentacene Units. *Chemistry of Materials* **2005**, *17*, 5024-5031. DOI: 10.1021/cm051150h.
- (12) Jones, A. C.; Kearns, N. M.; Ho, J.-J.; Flach, J. T.; Zanni, M. T. Impact of non-equilibrium molecular packings on singlet fission in microcrystals observed using 2D white-light microscopy. *Nature Chemistry* **2020**, *12*, 40-47. DOI: 10.1038/s41557-019-0368-9.

- (13) Illig, S.; Eggeman, A. S.; Troisi, A.; Jiang, L.; Warwick, C.; Nikolka, M.; Schweicher, G.; Yeates, S. G.; Henri Geerts, Y.; Anthony, J. E.; et al. Reducing dynamic disorder in small-molecule organic semiconductors by suppressing large-amplitude thermal motions. *Nature Communications* **2016**, *7*, 10736. DOI: 10.1038/ncomms10736.
- (14) Wong, C. Y.; Cotts, B. L.; Wu, H.; Ginsberg, N. S. Exciton dynamics reveal aggregates with intermolecular order at hidden interfaces in solution-cast organic semiconducting films. *Nature Communications* **2015**, *6*, 5946. DOI: 10.1038/ncomms6946.
- (15) Würthner, F. Perylene bisimide dyes as versatile building blocks for functional supramolecular architectures. *Chem. Commun.* **2004**, 1564-1579. DOI: 10.1039/b401630k.
- (16) Würthner, F.; Saha-Möller, C. R.; Fimmel, B.; Ogi, S.; Leowanawat, P.; Schmidt, D. Perylene Bisimide Dye Assemblies as Archetype Functional Supramolecular Materials. *Chemical Reviews* **2016**, *116*, 962-1052. DOI: 10.1021/acs.chemrev.5b00188.
- (17) Görl, D.; Zhang, X.; Stepanenko, V.; Würthner, F. Supramolecular block copolymers by kinetically controlled co-self-assembly of planar and core-twisted perylene bisimides. *Nature Communications* **2015**, *6*, 7009. DOI: 10.1038/ncomms8009.
- (18) Chen, S.; Slattum, P.; Wang, C.; Zang, L. Self-Assembly of Perylene Imide Molecules into 1D Nanostructures: Methods, Morphologies, and Applications. *Chem Rev* **2015**, *115*, 11967-11998. DOI: 10.1021/acs.chemrev.5b00312.
- (19) Boobalan, G.; Imran, P. M.; Ramkumar, S. G.; Nagarajan, S. Fabrication of luminescent perylene bisimide nanorods. *Journal of Luminescence* **2014**, *146*, 387-393. DOI: https://doi.org/10.1016/j.jlumin.2013.10.009.
- (20) Wilson-Kovacs, R. S.; Fang, X.; Hagemann, M. J. L.; Symons, H. E.; Faul, C. F. J. Design and Control of Perylene Supramolecular Polymers through Imide Substitutions. *Chemistry A European Journal* **2022**, *28*, e202103443. DOI: https://doi.org/10.1002/chem.202103443.
- (21) Wehner, M.; Würthner, F. Supramolecular polymerization through kinetic pathway control and living chain growth. *Nature Reviews Chemistry* **2019**, *4*, 38-53. DOI: 10.1038/s41570-019-0153-8.
- (22) Volek, T. S.; Armstrong, Z. T.; Sowa, J. K.; Wilson, K. S.; Bohlmann Kunz, M.; Bera, K.; Koble, M.; Frontiera, R. R.; Rossky, P. J.; Zanni, M. T.; et al. Structural Disorder at the Edges of Rubrene Crystals Enhances Singlet Fission. *J Phys Chem Lett* **2023**, *14*, 11497-11505. DOI: 10.1021/acs.jpclett.3c02845.
- (23) Zheng, Y.-Q.; Yao, Z.-F.; Lei, T.; Dou, J.-H.; Yang, C.-Y.; Zou, L.; Meng, X.; Ma, W.; Wang, J.-Y.; Pei, J. Unraveling the Solution-State Supramolecular Structures of Donor–Acceptor Polymers and their Influence on Solid-State Morphology and Charge-Transport Properties. *Advanced Materials* **2017**, *29*, 1701072. DOI: <a href="https://doi.org/10.1002/adma.201701072">https://doi.org/10.1002/adma.201701072</a>.
- (24) Paulino, V.; Cadena, D. M.; Liu, K.; Mukhopadhyay, A.; Roberts, S. T.; Olivier, J.-H. The Length of Molecular Tethers Can Be Used to Control the Structure and Electronic Properties of Stapled Supramolecular Polymers. *Chemistry of Materials* **2022**, *34*, 6518-6528. DOI: 10.1021/acs.chemmater.2c01353.
- (25) Ashcraft, A.; Liu, K.; Mukhopadhyay, A.; Paulino, V.; Liu, C.; Bernard, B.; Husainy, D.; Phan, T.; Olivier, J. H. A Molecular Strategy to Lock-in the Conformation of a Perylene Bisimide-Derived Supramolecular Polymer. *Angewandte Chemie International Edition* **2020**, *59*, 7487-7493. DOI: 10.1002/anie.201911780.
- (26) Sliz, R.; Czajkowski, J.; Fabritius, T. Taming the Coffee Ring Effect: Enhanced Thermal Control as a Method for Thin-Film Nanopatterning. *Langmuir: the ACS journal of surfaces and colloids* **2020**, *36*, 9562-9570. DOI: 10.1021/acs.langmuir.0c01560.
- (27) Diao, Y.; Shaw, L.; Bao, Z.; Mannsfeld, S. C. B. Morphology control strategies for solution-processed organic semiconductor thin films. *Energy Environ. Sci.* **2014**, 7, 2145-2159. DOI: 10.1039/c4ee00688g.
- (28) Yan, Q.; Cai, K.; Zhao, D. Supramolecular aggregates with distinct optical properties from PDI oligomers of similar structures. *Physical Chemistry Chemical Physics* **2016**, *18*, 1905-1910. DOI: 10.1039/c5cp05561j.
- (29) Li, H.; Zhang, Y.; Chen, B.; Wang, Y.; Teh, C.; Ng, G. H. B.; Meng, J.; Huang, Z.; Dong, W.; Tan, M. Y.; et al. J-Aggregation of

- Perylene Diimides in Silica Nanocapsules for Stable Near-Infrared Photothermal Conversion. *ACS Applied Bio Materials* **2019**, *2*, 1569-1577. DOI: 10.1021/acsabm.8b00839.
- (30) Oleson, A.; Zhu, T.; Dunn, I. S.; Bialas, D.; Bai, Y.; Zhang, W.; Dai, M.; Reichman, D. R.; Tempelaar, R.; Huang, L.; et al. Perylene Diimide-Based Hj- and hJ-Aggregates: The Prospect of Exciton Band Shape Engineering in Organic Materials. *The Journal of Physical Chemistry C* **2019**, *123*, 20567-20578. DOI: 10.1021/acs.jpcc.9b04429.
- (31) Liu, S.-G.; Sui, G.; Cormier, R. A.; Leblanc, R. M.; Gregg, B. A. Self-Organizing Liquid Crystal Perylene Diimide Thin Films: Spectroscopy, Crystallinity, and Molecular Orientation. *The Journal of Physical Chemistry B* **2002**, *106*, 1307-1315. DOI: 10.1021/jp013254v.
- (32) Belova, V.; Wagner, B.; Reisz, B.; Zeiser, C.; Duva, G.; Rozbořil, J.; Novák, J.; Gerlach, A.; Hinderhofer, A.; Schreiber, F. Real-Time Structural and Optical Study of Growth and Packing Behavior of Perylene Diimide Derivative Thin Films: Influence of Side-Chain Modification. *The Journal of Physical Chemistry C* 2018, 122, 8589-8601. DOI: 10.1021/acs.jpcc.8b00787.
- (33) Zhang, F.; Ma, Y.; Chi, Y.; Yu, H.; Li, Y.; Jiang, T.; Wei, X.; Shi, J. Self-assembly, optical and electrical properties of perylene diimide dyes bearing unsymmetrical substituents at bay position. *Scientific Reports* **2018**, *8*. DOI: 10.1038/s41598-018-26502-5.
- (34) Zugenmaier, P.; Duff, J.; Bluhm, T. L. Crystal and Molecular Structures of Six Differently with Halogen Substituted Bis (benzylimido) perylene. *Crystal Research and Technology* **2000**, *35*, 1095-1115. DOI: <a href="https://doi.org/10.1002/1521-4079(200009)35:9<1095::AID-CRAT1095>3.0.CO;2-5">https://doi.org/10.1002/1521-4079(200009)35:9<1095::AID-CRAT1095>3.0.CO;2-5</a>.
- (35) Hadicke, E.; Graser, F. Structures of eleven perylene-3,4:9,10-bis(dicarboximide) pigments. *Acta Crystallographica Section C* **1986**, 42, 189-195. DOI: doi:10.1107/S0108270186096828.
- (36) Davydova, D. y.; de la Cadena, A.; Akimov, D.; Dietzek, B. Transient absorption microscopy: advances in chemical imaging of photoinduced dynamics. *Laser & Photonics Reviews* **2016**, *10*, 62-81. DOI: <a href="https://doi.org/10.1002/lpor.201500181">https://doi.org/10.1002/lpor.201500181</a>.
- (37) Fischer, M. C.; Wilson, J. W.; Robles, F. E.; Warren, W. S. Invited Review Article: Pump-probe microscopy. *Rev Sci Instrum* **2016**, *87*, 031101. DOI: 10.1063/1.4943211.
- (38) Huang, L.; Wong, C.; Grumstrup, E. Time-Resolved Microscopy: A New Frontier in Physical Chemistry. *The Journal of Physical Chemistry A* **2020**, *124*, 5997-5998. DOI: 10.1021/acs.jpca.0c05511.
- (39) Piland, G.; Grumstrup, E. M. High-Repetition Rate Broadband Pump-Probe Microscopy. *The Journal of Physical Chemistry A* **2019**, *123*, 8709-8716. DOI: 10.1021/acs.jpca.9b03858.
- (40) Dean, J. C.; Oblinsky, D. G.; Rafiq, S.; Scholes, G. D. Methylene Blue Exciton States Steer Nonradiative Relaxation: Ultrafast Spectroscopy of Methylene Blue Dimer. *The Journal of Physical Chemistry B* **2016**, *120*, 440-454. DOI: 10.1021/acs.jpcb.5b11847.
- (41) Verma, S.; Ghosh, A.; Das, A.; Ghosh, H. N. Ultrafast Exciton Dynamics of J- and H-Aggregates of the Porphyrin-Catechol in Aqueous Solution. *The Journal of Physical Chemistry B* **2010**, *114*, 8327-8334. DOI: 10.1021/jp101643c.
- (42) Kakade, S.; Ghosh, R.; Palit, D. K. Excited State Dynamics of Zinc–Phthalocyanine Nanoaggregates in Strong Hydrogen Bonding Solvents. *The Journal of Physical Chemistry C* **2012**, *116*, 15155-15166. DOI: 10.1021/jp304369r.
- (43) Caplins, B. W.; Mullenbach, T. K.; Holmes, R. J.; Blank, D. A. Intermolecular Interactions Determine Exciton Lifetimes in Neat Films and Solid State Solutions of Metal-Free Phthalocyanine. *The Journal of Physical Chemistry C* **2015**, *119*, 27340-27347. DOI: 10.1021/acs.jpcc.5b09817.
- (44) Vauthey, E. Photoinduced Symmetry-Breaking Charge Separation. *ChemPhysChem* **2012**, *13*, 2001-2011. DOI: 10.1002/cphc.201200106.
- (45) Koch, M.; Myahkostupov, M.; Oblinsky, D. G.; Wang, S.; Garakyaraghi, S.; Castellano, F. N.; Scholes, G. D. Charge Localization after Ultrafast Photoexcitation of a Rigid Perylene Perylenediimide Dyad Visualized by Transient Stark Effect. *Journal of the American Chemical Society* **2017**, *139*, 5530-5537. DOI: 10.1021/jacs.7b01630.

- (46) Leonhardt, H.; Weller, A. DOI: 10.1524/zpch.1961.29.3 4.277.
- (47) Sundström, V.; Gillbro, T. Excited state dynamics and photophysics of aggregated dye chromophores in solution. *The Journal of Chemical Physics* **1985**, *83*, 2733-2743. DOI: 10.1063/1.449275.
- (48) Huff, J. S.; Davis, P. H.; Christy, A.; Kellis, D. L.; Kandadai, N.; Toa, Z. S. D.; Scholes, G. D.; Yurke, B.; Knowlton, W. B.; Pensack, R. D. DNA-Templated Aggregates of Strongly Coupled Cyanine Dyes: Nonradiative Decay Governs Exciton Lifetimes. *The Journal of Physical Chemistry Letters* **2019**, *10*, 2386-2392. DOI: 10.1021/acs.jpclett.9b00404.
- (49) Jones, A. C.; Kearns, N. M.; Ho, J. J.; Flach, J. T.; Zanni, M. T. Impact of non-equilibrium molecular packings on singlet fission in microcrystals observed using 2D white-light microscopy. *Nat Chem* **2020**, *12*, 40-47. DOI: 10.1038/s41557-019-0368-9.
- (50) Brown, K. E.; Salamant, W. A.; Shoer, L. E.; Young, R. M.; Wasielewski, M. R. Direct Observation of Ultrafast Excimer Formation in Covalent Perylenediimide Dimers Using Near-Infrared Transient Absorption Spectroscopy. *The Journal of Physical Chemistry Letters* **2014**, *5*, 2588-2593. DOI: 10.1021/jz5011797.
- (51) Heckelmann, I.; Lu, Z.; Prentice, J. C. A.; Auras, F.; Ronson, T. K.; Friend, R. H.; Nitschke, J. R.; Feldmann, S. Supramolecular Self-Assembly as a Tool To Preserve the Electronic Purity of Perylene Diimide Chromophores\*\*. *Angewandte Chemie International Edition* **2023**, *62*. DOI: 10.1002/anie.202216729.
- (52) Giaimo, J. M.; Lockard, J. V.; Sinks, L. E.; Scott, A. M.; Wilson, T. M.; Wasielewski, M. R. Excited Singlet States of Covalently Bound, Cofacial Dimers and Trimers of Perylene-3,4:9,10-bis(dicarboximide)s. *The Journal of Physical Chemistry A* **2008**, *112*, 2322-2330. DOI: 10.1021/jp710847q.
- (53) Schubert, A.; Settels, V.; Liu, W.; Würthner, F.; Meier, C.; Fink, R. F.; Schindlbeck, S.; Lochbrunner, S.; Engels, B.; Engel, V. Ultrafast Exciton Self-Trapping upon Geometry Deformation in Perylene-Based Molecular Aggregates. *The Journal of Physical Chemistry Letters* **2013**, *4*, 792-796. DOI: 10.1021/jz4000752.
- (54) Ginsberg, N. S.; Tisdale, W. A. Spatially Resolved Photogenerated Exciton and Charge Transport in Emerging

- Semiconductors. *Annual Review of Physical Chemistry* **2020**, *71*, 1-30. DOI: 10.1146/annurev-physchem-052516-050703.
- (55) Hickey, C. L.; Grumstrup, E. M. Reduced Artifact Approach for Determining Diffusion Coefficients in Time-Resolved Microscopy. *The Journal of Physical Chemistry C* **2020**, *124*, 14016-14021. DOI: 10.1021/acs.jpcc.0c02302.
- (56) Zhu, T.; Wan, Y.; Huang, L. Direct Imaging of Frenkel Exciton Transport by Ultrafast Microscopy. *Accounts Chem Res* **2017**, *50*, 1725-1733. DOI: 10.1021/acs.accounts.7b00155.
- (57) Pandya, R.; Chen, R. Y. S.; Gu, Q.; Gorman, J.; Auras, F.; Sung, J.; Friend, R.; Kukura, P.; Schnedermann, C.; Rao, A. Femtosecond Transient Absorption Microscopy of Singlet Exciton Motion in Side-Chain Engineered Perylene-Diimide Thin Films. *J Phys Chem A* **2020**, *124*, 2721-2730. DOI: 10.1021/acs.jpca.0c00346.
- (58) Miller, A.; Abrahams, E. Impurity Conduction at Low Concentrations. *Physical Review* **1960**, *120*, 745-755. DOI: 10.1103/physrev.120.745.
- (59) Geng, Y.; Li, H.-B.; Wu, S.-X.; Su, Z.-M. The interplay of intermolecular interactions, packing motifs and electron transport properties in perylene diimide related materials: a theoretical perspective. *Journal of Materials Chemistry* **2012**, *22*, 20840. DOI: 10.1039/c2jm33369d.
- (60) Balzer, D.; Smolders, T.; Blyth, D.; Hood, S. N.; Kassal, I. Delocalised kinetic Monte Carlo for simulating delocalisation-enhanced charge and exciton transport in disordered materials. *Chem Sci* **2020**, *12*, 2276-2285. DOI: 10.1039/d0sc04116e.
- (61) Mesta, M.; Carvelli, M.; de Vries, R. J.; van Eersel, H.; van der Holst, J. J. M.; Schober, M.; Furno, M.; Lüssem, B.; Leo, K.; Loebl, P.; et al. Molecular-scale simulation of electroluminescence in a multilayer white organic light-emitting diode. *Nature Materials* **2013**, *12*, 652-658. DOI: 10.1038/nmat3622.